

Predictability problem in dynamical systems and in chaotic climate dynamics

A. Bershadskii

ICAR, P.O. Box 31155, Jerusalem 91000, Israel

Predictability horizon properties of chaotic dynamical systems can be related to their spectral properties. It is shown, using this relationship, that the spectral properties of the leading large-scale climate daily indices indicate a smooth predictability: i.e. their intrinsic predictability horizons can be indefinitely extended by reducing the initial error. Special properties of the Madden-Julian Oscillation have been also discussed in this context.

POWER SPECTRUM AND PREDICTABILITY

A simple and assured way to distinguish between chaotic and quasi-periodic dynamics is to study power spectrum of the time signals generated by the dynamical systems. For chaotic systems the power spectrum will be a *broadband* one. Figure 1, for instance shows a power spectrum computed for z -component of the Lorenz equations [1].

$$\frac{dx}{dt} = \sigma(y - x), \quad \frac{dy}{dt} = rx - y - xz, \quad \frac{dz}{dt} = xy - bz \quad (1)$$

for the parameters The $b = 8/3$, $\sigma = 10.0$ and $r = 28.0$. The power spectrum was computed by the maximum entropy method (with an optimal resolution [2]). The *broadband* spectrum decays exponentially with frequency (dashed straight line in the semi-log scales)

$$E(f) \propto \exp(-f/f_c) \quad (2)$$

It is also true for many other dynamical systems with the chaotic behaviour (including some atmospheric phenomena) [2]-[6]. This spectral decay can be related to the *smooth* sensitivity to the initial conditions mentioned by E. N. Lorenz in his 1969 paper [7]:

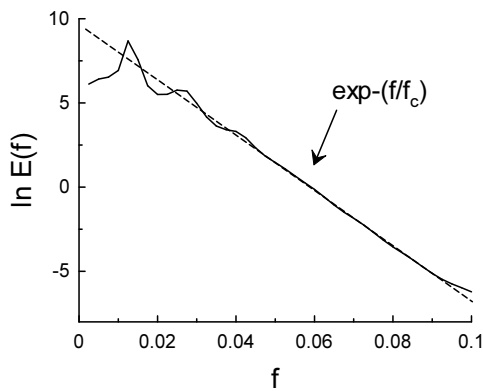


FIG. 1: Logarithm of power spectrum vs. frequency f . The dashed straight line indicates Eq. (2).

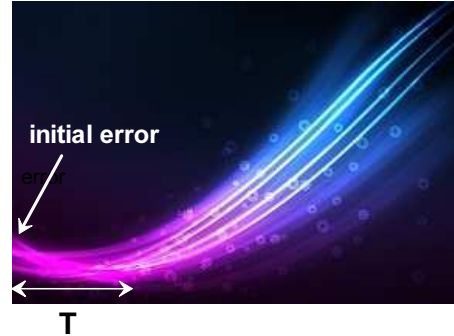


FIG. 2: A sketch of the trajectories development.

”The error eventually becomes much larger than the initial error. At any particular future time the error may be made arbitrarily small by making the initial error sufficiently small, but, no matter how small the initial error (if not zero), the error becomes large in the sufficiently distant future.”

The initial error (say an ε -ball in the phase space, with the initial state of the trajectory as its center) is a measure of the differences in the initial conditions. The above mentioned smoothness of the chaotic behaviour is naturally related to the predictability problem (predictability horizon properties). Figure 2 shows a sketch of development of the trajectories of a chaotic system. For the smooth case one can make the time of controlled behaviour \mathbf{T} arbitrary large (but still finite) by reducing the initial error. The \mathbf{T} can be also considered as a predictability horizon.

Some trajectories starting from the error’s ε -ball can violate the controlled behaviour, but measure corresponding to these trajectories will be zero.

Let us define (following the Ref. [7]) a *smooth* and a *rough* predictability. At smooth predictability the predictability horizon can be indefinitely extended by reducing the initial error.

At *rough* predictability the predictability horizon cannot be indefinitely extended by reducing the initial error.

The Lorenz system Eq. (1), for instance, has the smooth predictability and the exponential spectral decay Fig. 1. This relationship can be generalized for a wide class of the chaotic systems. Namely, the chaotic systems with the smooth sensitivity to the initial conditions (the smooth predictability) have a stretched exponential spectral decay:

$$E(f) \propto \exp -(f/f_0)^\beta \quad (3)$$

where $\beta \leq 1$. Moreover, for the chaotic systems with the rough predictability the spectral decay has a power-law form

$$E(f) \propto f^{-\gamma} \quad (4)$$

This dependence of the spectral decay on the smoothness resembles relation between smoothness and truncation of the Fourier transform to finite interval (do not confuse the smoothness of a trajectory itself and the above described Lorenz's smoothness of the collective trajectories evolution in the phase space).

For the smooth Hamiltonian systems (in the Lorenz sense) only two values of the parameter β are possible $\beta = 3/4$ and $\beta = 1/2$ [8] (but it should be noted that not all chaotic Hamiltonian systems have the spectral decay in the form of the Eq. (3) or Eq. (4)).

Appearance of the stretched exponential spectrum Eq. (3) is a good indicator of the smooth predictability, whereas the power-law spectrum Eq. (4) indicates the rough predictability (cf. the recent reviews Refs. [9]-[14] and next Section).

HAMILTONIAN DYNAMICAL SYSTEMS

Let us consider two examples of the Hamiltonian dynamical systems - one with smooth and another with rough chaotic behaviour.

A. Classic Toda lattice.

The classic Toda lattice is a one dimensional N -particle Hamiltonian dynamical system having an exponentially decaying (with the distance between the particles) potential [15]. This dynamical system is completely integrable.

Figure 3 shows spectral data taken from Ref. [16], where the direct numerical simulations were performed for the classic Toda lattice on a ring with zero total momentum, periodic boundary conditions and random initial conditions. The appropriate scales were chosen for the Fig. 3 to indicate the stretched exponential decay Eq. (3) with $\beta \simeq 3/4$ (the straight line).

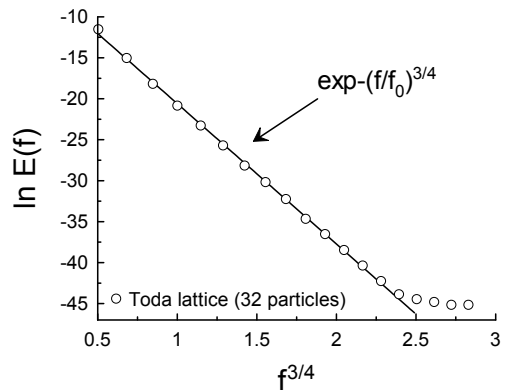


FIG. 3: A decaying part of the power spectrum of the q_1 coordinate for the classic Toda lattice.

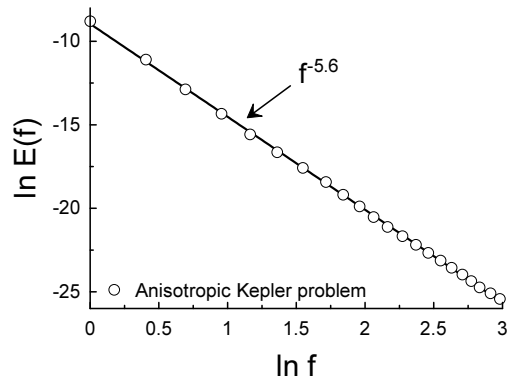


FIG. 4: A decaying part of the power spectrum of the z_1 coordinate for the anisotropic Kepler problem.

B. Anisotropic Kepler system.

The anisotropic Kepler problem describes the motion of an electron in an anisotropic crystal (in the Coloumb field) [17]. Its effective mass is different along the z -direction and x - y plane. In the anisotropic case the system is non-integrable.

Figure 4 shows spectral data taken from Ref. [18], where the direct numerical simulations were performed for the anisotropic Kepler problem. The appropriate scales were chosen for the Fig. 4 to indicate the power-law decay Eq. (4) with $\gamma \simeq 5.6$ (the straight line).

In the Refs. [14] and [19] one can find an interesting discussion on the subject and in the Refs. [20]-[23] the evidences of the relevance of the Hamiltonian dynamics to the climate.

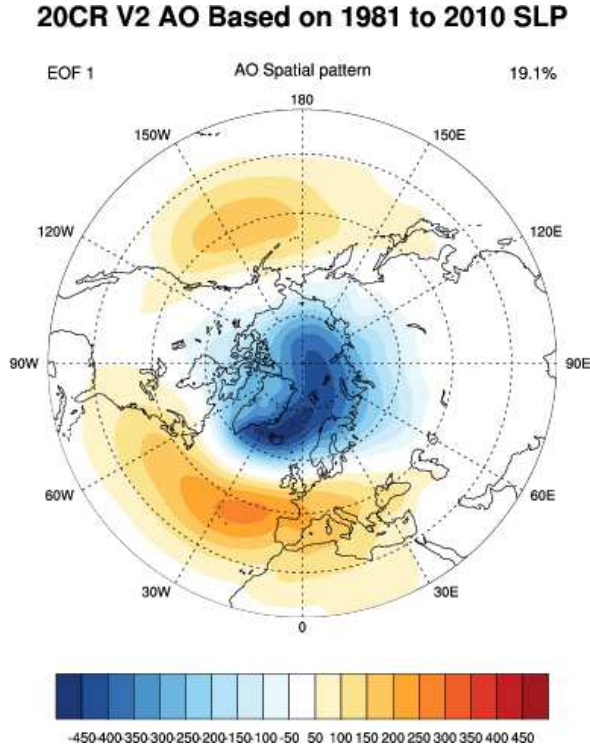


FIG. 5: Spatial pattern of the Arctic Oscillation [26].

LARGE-SCALE CLIMATE DYNAMICS

Let us start from the Arctic Oscillation. The Arctic Oscillation (AO index) is a primary annular mode of extratropical atmospheric circulation in the Northern Hemisphere [24],[25]. It represents a pressure gradient between the polar and subpolar regions.

At the site [26] the *sea-level* pressure (SLP) based AO and AAO daily indices were calculated for a prolonged time period. The SLP is the atmospheric pressure at sea level at a given location. If a station is not located at sea level the SLP is a correction of the station pressure to corresponding sea level (taking into account the variation of pressure with height and influence of temperature).

Figure 5 shows a spatial pattern of the Arctic Oscillation. The Empirical Orthogonal Function (EOF) is based on 1981-2010yy monthly anomalies of SLP poleward of 20°N (the 20CR V2 dataset) [26]. The AO daily index was obtained by projecting the daily anomalies of SLP onto the EOF's.

Figure 6 shows power spectrum computed for the daily AO index for period 1932-2012yy (the timeseries were taken from the site [26]). The power spectrum was computed by the maximum entropy method (with an optimal resolution [2]). The straight line indicates correspondence to the Eq. (3) with $\beta = 3/4$.

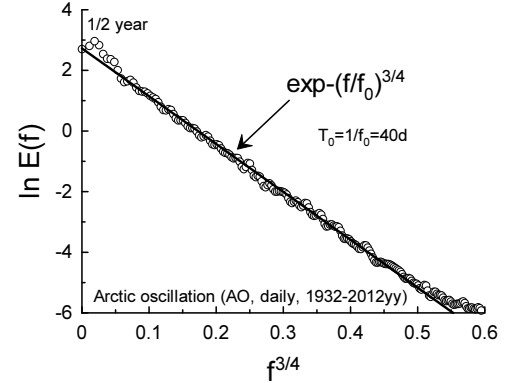


FIG. 6: Power spectrum of the AO daily SLP index for the period 1932-2012yy. The data for computation were taken from the site [26].

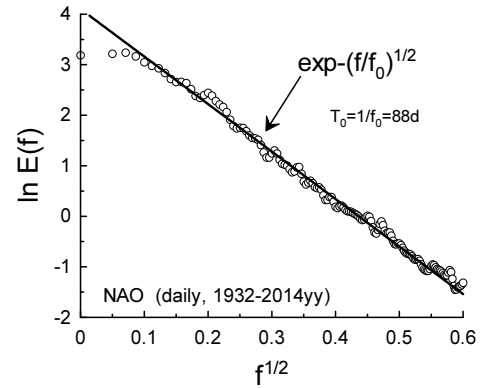


FIG. 7: Power spectrum of the NAO daily SLP index for the period 1932-2014yy. The data for computation were taken from the site [27].

The southern counterpart of the Arctic Oscillation - the Antarctic Oscillation (AAO) exhibit analogous spectral properties (but with $\beta \simeq 1/2$). Although the corresponding data for the AAO daily index are less reliable.

Figure 7 shows power spectrum computed for the North Atlantic Oscillation (NAO) daily SLP index for period 1932-2014yy (the timeseries were taken from the site [27], see also Ref. [28] for more details about the data acquisition). For a comprehensive review of the North Atlantic Oscillation properties see Ref. [29].

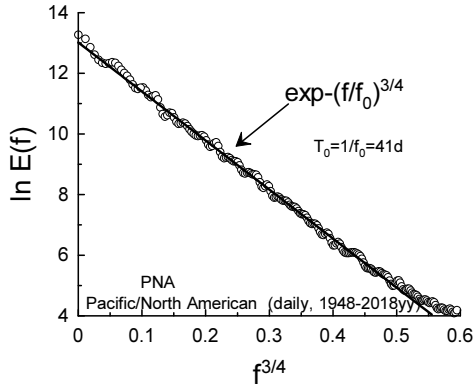


FIG. 8: Power spectrum of the PNA daily index for the period 1948-2018yy. The data for computation were taken from the site [30].

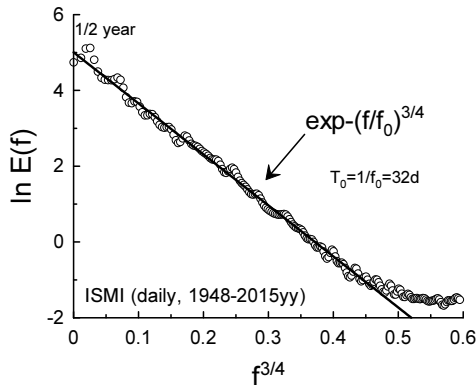


FIG. 9: Power spectrum of the intraseasonal daily ISM index for the period 1948-2015yy. The data for computation were taken from the site [32].

Figure 8 shows power spectrum computed for the Pacific/North American (PNA) daily index for period 1948-2018yy (the timeseries were taken from the site [30]). The computations of the PNA daily index were made for 500mb height oscillating patterns (one can find more details of the NCEP-NCAR R1 reanalysis in Ref. [31]).

Figure 9 shows power spectrum computed for the intraseasonal (i.e. after subtraction of the interannual variability and annual cycle) daily Indian Summer Monsoon (ISM) index for the period 1948-2015yy (the timeseries were taken from the site [32]). A compre-

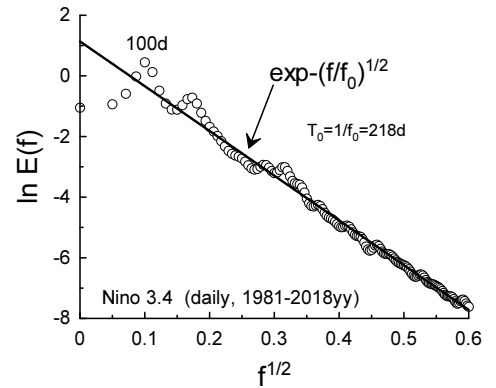


FIG. 10: Power spectrum of the daily Nino 3.4 index for the period 1981-2018yy. The data for computation were taken from the site [34].

hensive review of the Monsoon properties can be found in Ref. [33]. Analogous situation takes also place for the complimentary Western North Pacific Monsoon (WNPM) intraseasonal daily index as well as for their equatorial counterpart the Australian Monsoon.

Figure 10 shows power spectrum computed for the intraseasonal (i.e. after subtraction of the interannual variability and annual cycle) daily Niño 3.4 index characterizing the El Niño/La Niña phenomenon. The index is based on SST anomalies averaged across the Niño 3.4 region in the east-central Equatorial Pacific (the timeseries were taken from the site [34]). The Niño 3.4 index is the most commonly used index to describe El Niño/La Niña events [35].

One can see that for the leading large-scale climate oscillations (patterns) the decaying part of the power spectrum is a stretched exponential Eq. (3) (with the Hamiltonian values of the $\beta \simeq 3/4$ or $\beta \simeq 1/2$), that indicates the smooth predictability (it should be noted that the daily global temperature anomalies also belong to this class [36]). Only for one important large-scale climate oscillation - Madden-Julian Oscillation or MJO (the RMM and VPM daily indices [37],[38]) the decaying part of the power spectrum has a power law - Eq. (4) (with $\gamma \simeq 3$) [8].

MADDEN-JULIAN OSCILLATION

A sketch (by Fiona Marti, adapted from Ref. [39]) of the surface and upper-atmosphere formation of the Madden-Julian Oscillation (MJO) is shown in figure

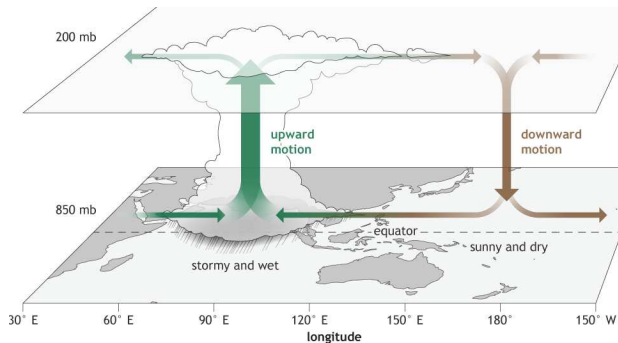


FIG. 11: A sketch of the surface and upper-atmosphere formation of the MJO.

11. The enhanced convective phase (the thunderstorm cloud) is concentrated over the Indian Ocean while the suppressed convective phase dominates atmosphere over the west-central Pacific Ocean. Traversing the planet in eastward direction this formation returns with an average period near 50 days. It is a planetary-scale coupled recurring pattern in baroclinic circulation and deep convection [38],[40]. The MJO has strong influence on extratropical weather and climate through its global teleconnections [41]-[47].

Two daily indices RMM1 and RMM2 (representing two principal components [37]) are now widely used for the predicting and monitoring purposes related to the MJO dynamics. The RMM indices are based on a pair of EOFs of the near-equatorially (averaged) fields: the satellite-observed OLR (outgoing long-wave radiation), 850-hPa zonal wind and 200-hPa zonal wind. The indices were computed by projection of the data onto the EOFs (the interannual variability and annual cycle were removed from the time series [37]). Figure 12 shows power spectrum computed for the daily RMM1 index for period 1979-2017yy (the data - time series, were taken from the site [34]). The straight line indicates correspondence to the Eq. (4) with $\gamma \simeq 3$.

Therefore, unlike all the other above mentioned large-scale climate oscillations, the MJO (represented by the RMM1 index) should have rough predictability. For RMM2 index and for the complimentary daily indices - VPM1 and VPM2 the situation is similar (see the Ref. [8] for more details).

But the situation can be easily improved in this case. The power law decay observed in the Fig. 12 and the corresponding rough type of the predictability can be considered as a result of a random noise produced by

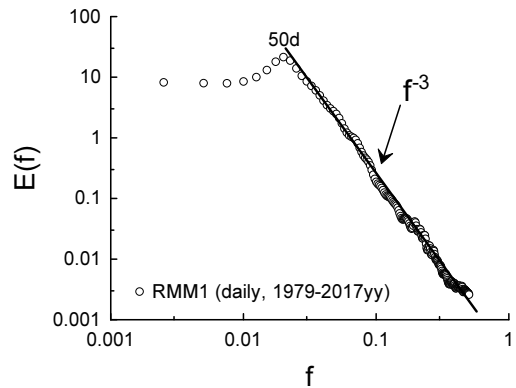


FIG. 12: Power spectrum of the RMM1 daily index for the period 1979-2017yy. The data for computation were taken from the site [34].

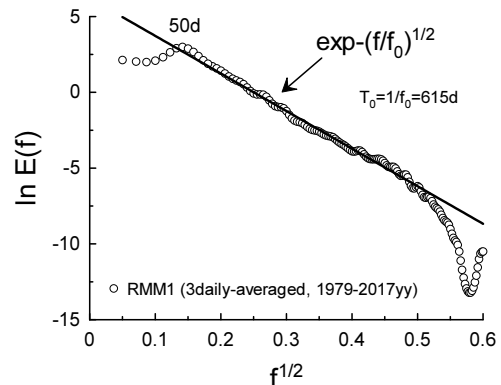


FIG. 13: Power spectrum of the daily RMM1 index smoothed by the three days running average.

the high frequency waves. Such waves are common for the tropics (see, for instance, Ref. [48] and references therein). The average period of these waves is less than three days [48]. Therefore, using a simple (smoothing) filter - three days running average, we can remove the random influence of these waves on the daily time series RMM1, RMM2, VPM1 and VPM2 (cf. the Ref. [8]). Figure 13 shows power spectrum computed for the smoothed (filtered) daily RMM1 index. The straight line indicates correspondence to the Eq. (3) with $\beta = 1/2$ (one of the Hamiltonian values). For the other MJO indices - RMM2, VPM1 and VPM2 the situation is similar (cf. the Ref. [8]).

ACKNOWLEDGEMENT

I thank O. Adam, B. Galperin, Y.C. Li, A. Pikovsky and participants of the "Climate, Atmosphere and Ocean" seminar (HUJI) for stimulating discussions. I acknowledge use of the data provided by the Earth system research laboratory (NOAA), the Zenodo database (CERN), the KNMI Climate Explorer (Netherlands) and the Asia-Pacific Data Research Center at the University of Hawaii.

-
- [1] E.N. Lorenz, *J. Atmos. Sci.*, **20**, 130 (1963).
 [2] N. Ohtomo, K. Tokiwano, Y. Tanaka et. al., *J. Phys. Soc. Jpn.* **64** 1104 (1995).
 [3] J. D. Farmer, *Physica D*, **4**, 366 (1982).
 [4] D.E. Sigeti, *Phys. Rev. E*, **52**, 2443 (1995).
 [5] A. Bershadskii, *EPL*, **88**, 60004 (2009).
 [6] S.M. Osprey and M.H.P. Ambaum, *Geophys. Res. Lett.* **38**, L15702 (2011).
 [7] E.N. Lorenz, *Tellus*, **XXI** (3), 289 (1969).
 [8] A. Bershadskii, arXiv:1805.06820; arXiv:1803.10139 (2018).
 [9] M. Ghil et al., *Reviews of Geophysics*, **40**, 1 (2002).
 [10] T.N Palmer, A Doring and G Seregin, *Nonlinearity*, **27**, R123 (2014).
 [11] N.P. Wedi, *Phil. Trans. R. Soc. A*, **372**, 20130289 (2014).
 [12] S. Vannitsem, *Chaos* **27**, 032101 (2017).
 [13] T.Y. Leung, et al., *Geophys. Res. Abstracts*, **20**, EGU2018-371 (2018).
 [14] Y.C. Li, *Comm. in Nonlinear Science and Numerical Simulation*, **70**, 74 (2019).
 [15] M. Toda, *Theory of Nonlinear Lattices*, 2nd Ed. Springer, Berlin (1989).
 [16] T.A. Elsayed, B. Hess and B.V. Fine, *Phys. Rev. E*, **90**, 022910 (2014).
 [17] K. Ramasubramanian and M. Sriram, *Physica D*, **139**, 72 (2000).
 [18] T.A. Elsayed, Dr.Sc. Thesis (2013).
<http://archiv.ub.uni-heidelberg.de/volltextserver/15648/1/thesis%20tarek%20elsayed.pdf>
 [19] J. Lighthill, *Proc. R. Soc. Lond. A*, **407**, 35 (1986).
 [20] T.G. Shepherd, *Advances in Geophysics*, **32**, 287 (1990).
 [21] T.G. Shepherd, *Encyclopedia of Atmospheric Sciences*, J. R. Holton et al., Ed., 929 (Academic Press, 2003).
 [22] V. Pelino et al., *Commun. Nonlinear Sci. Numer. Simulat.*, **17**, 2122 (2012).
 [23] A. Gluhovsky, and K. Grady, *Chaos*, **26**, 023119 (2016).
 [24] D.W.J. Thompson and J.M. Wallace, *J. Clim.*, **13**, 1000 (2000).
 [25] J.M Wallace, On the role of the Arctic and Antarctic oscillations in polar climate. ECMWF Seminar on Polar Meteorology (2006). Available at the site: <https://www.ecmwf.int>
 [26] <https://www.esrl.noaa.gov/psd/data/20thC-Rean/timeseries/daily/AO/>
 [27] T. Cropper et al., <http://doi.org/10.5281/zenodo.9979>
 [28] T. Cropper et al., *Geosci. Data J.*, **2**, 12 (2015).
 [29] J.W. Hurrell et al., in *The North Atlantic Oscillation: Climatic Significance and Environmental Impact*, Geophysical Monograph 134, p.1, American Geophysical Union (2003).
 [30] <https://www.esrl.noaa.gov/psd/data/timeseries/daily/PNA>
 [31] E. Kalnay et al., *Bull. Amer. Meteor. Soc.*, **77**, 437 (1996).
 [32] <http://apdrc.soest.hawaii.edu/projects/monsoon/>
 [33] B. Wang, R. Wu and K.-M. Lau, *J. Climate*, **14**, 4073 (2001).
 [34] <https://climexp.knmi.nl/start.cgi>
 [35] <https://www.ncdc.noaa.gov/teleconnections/enso/indicators/sst/>
 [36] A. Bershadskii, arXiv:1806.01750 (2018).
 [37] M.C. Wheeler and H.H. Hendon, *Monthly Weather Review*, **132**, 1917 (2004).
 [38] M.J. Ventrice et al., *Monthly Weather Review*, **141**, 4197 (2013).
 [39] <https://www.climate.gov/news-features/blogs/enso/what-mjo-and-why-do-we-care>
 [40] C. Zhang, *Rev. Geophys.*, **43**, 1 (2005).
 [41] C. Stan et al., *Rev. Geophys.*, **55**, 902 (2017).
 [42] C. Cassou, *Nature*, **455**, 523 (2008).
 [43] W.K.M. Lau, in *Intraseasonal Variability of the Atmosphere-Ocean Climate System* (W.K.M. Lau and D.E. Waliser, Eds., Springer), 277 (2005).
 [44] H.H. Hendon, M.C. Wheeler and C. Zhang, *J. Climate*, **20**, 531 (2007).
 [45] C. Zhang, in *Encyclopedia of Atmospheric Sciences*, 73 (Elsevier, second edition 2015).
 [46] F. Vitart, *Quart. J. Roy. Met. Soc.*, **143**, 2210 (2017).
 [47] C. Schwartz and C.I. Garfinkel, *J. Geophys. Res.: Atmospheres*, **122**, 4184 (2017).
 [48] S.N. Tulich and G.N. Kiladis, *J. Atmos. Sci.*, **69**, 2995 (2012).